

Hydrodynamic Stability of Hypersonic Chemically Reacting Boundary Layers I

Olaf Marxen

Department of Mechanical Engineering Sciences
Faculty of Engineering and Physical Sciences
University of Surrey
Guildford, Surrey GU2 7XH
United Kingdom

o.marxen@surrey.ac.uk

ABSTRACT

In these notes, an introduction to linear hydrodynamic instability in the presence of high-temperature gas effects is given. Focus is put on the effect of chemical reactions on the boundary layer and its linear instability. Results have been obtained from numerical simulations of configurations in which the temperature at the boundary-layer edge is low, whereas the temperature inside the boundary layer may be very high.

Due to endothermic dissociation reactions occurring close to the wall, the near-wall temperature is lower in the case of chemical reactions. This reduction of temperature close to the wall also causes a reduction in viscosity in the near-wall region, which in turn causes the velocity boundary layer to be thinner. For moderately reactive flows, the effect of chemical reactions is indeed found to be very similar to the effect of cooling at the wall. This holds for both the mean flow and the evolution of small-amplitude perturbations. For strongly reacting flows including those in local thermodynamic equilibrium, the effect of reactions is more complex.

Amplification rates as well as amplitude and phase functions from direct numerical simulations compare favorably with those obtained from linear stability theory, although such an agreement is certainly not perfect.

Contents

1.0 Introduction	2
1.1 Hypersonic High-Temperature Boundary-Layer Flows	3
1.1.1 High-Temperature Gas Effects	3
1.1.2 Vehicle Configurations	5
1.1.3 Numerical Methods for Flows with High-Temperature Gas Effects	5
1.2 Introduction to Laminar-Turbulent Transition	5
1.2.1 Laminar and Turbulent Boundary Layers	6
1.2.2 The Three Stages of the Transition Process	6
1.2.3 Transition in Hypersonic High-Temperature Boundary Layers	7
1.3 Introduction to Linear Boundary-Layer Instability	8
1.3.1 Linear Stability Theory and Eigenvalue spectra	8

1.3.2	Non-Parallel Effects	9
1.3.3	Instability of Traveling Waves	9
1.3.4	Parametric Effects	10
1.4	Scope	11
2.0	Base Flow	12
2.1	High-Temperature Gas Effects in a Flat-Plate Boundary Layer at Mach 10	12
2.2	The Effect of Freestream Temperature	13
3.0	Linear Disturbance Evolution in Hypersonic Flow	14
3.1	High-Temperature Gas Effects in a Flat-Plate Boundary Layer at Mach 10	16
3.2	The Effect of Freestream Temperature	18
3.3	Comparison between DNS and Linear Stability Theory	19

1.0 INTRODUCTION

The viscous flow around a body will lead to the development of a momentum boundary layer if the viscous forces are small compared to the inertial forces. In this case, the *Reynolds number* is large and the direct influence of viscosity is restricted to an area close to the body, the boundary layer. In order to calculate the Reynolds number as well as other non-dimensional numbers for boundary layers, reference values are usually taken in the freestream (marked by the subscript ∞ below). Here, all dimensional quantities are marked by a modifier ($\tilde{}$), and we have the following reference quantities: temperature $\tilde{T}_{ref} = (\gamma_\infty - 1)\tilde{T}_\infty$, density $\tilde{\rho}_\infty$, specific heat ratio $\gamma_\infty = \tilde{c}_{p,\infty} / \tilde{c}_{v,\infty}$, thermal conductivity \tilde{k}_∞ , and viscosity $\tilde{\mu}_\infty$. The reference velocity is the speed of sound \tilde{c}_∞ , and we have chosen a reference length \tilde{L}_{ref} . The main geometry under consideration here is a semi-infinite flat plate and hence no single length scale is present, which makes the choice of the reference length arbitrary. We will therefore often use the distance x from the leading edge of the plate to normalize our results. The chosen quantities yield a reference time $\tilde{t}_{ref} = \tilde{L}_{ref} / \tilde{c}_\infty$ and a reference pressure $\tilde{p}_{ref} = \tilde{\rho}_\infty \tilde{c}_\infty^2$. With these quantities, the Reynolds number Re_∞ can be defined as:

$$Re_\infty = \tilde{\rho}_\infty \tilde{c}_\infty \tilde{L}_{ref} / \tilde{\mu}_\infty . \tag{1}$$

Similarly, for problems in which the temperature between the outer flow and the surface of the body differs significantly, low thermal diffusivity may lead to the development of a thermal boundary layer. The non-dimensional *Prandtl number* Pr_∞ reflects the relative thickness of the momentum and thermal boundary layers:

$$Pr_\infty = \tilde{\mu}_\infty \tilde{c}_{p,\infty} / \tilde{k}_\infty . \tag{2}$$

Another central non-dimensional parameter is the *Mach number* Ma_∞ , which is defined as the ratio between the freestream velocity and the reference speed of sound:

$$Ma_\infty = \tilde{u}_\infty / \tilde{c}_\infty . \tag{3}$$

Incompressible flows possess a vanishing Mach number, and this number remains below one for subsonic flows. For supersonic flow, the Mach number is larger than one at least in the freestream for boundary layers. A clear distinction between supersonic and hypersonic flow does not exist, as both possess a Mach number larger than one. Here, we regard hypersonic flow as the very supersonic flow in which additional effects, such as

chemical reactions, strong shock waves, or ionization occur. Typically, this happens only if the Mach number is much larger than one, either in the freestream or upstream of a strong shock wave.

For gases with high-temperature gas effects, we need to consider an additional non-dimensional number. This number, the *Eckert number* Ec_∞ , measures the ratio of kinetic energy and enthalpy. In our definition, it is divided by the Mach number and hence it uses the freestream speed of sound in the numerator. It provides a direct measure for the deviation from a calorically perfect gas behavior in the freestream. If this number is equal to one, then the flow in the freestream behaves as a calorically perfect gas. In essence, in our definition the Eckert number corresponds to the ratio of the actual gas constant \tilde{R} and the gas constant for a corresponding calorically perfect gas:

$$Ec_\infty = \tilde{c}_\infty^2 / \left(\tilde{c}_{p,\infty} (\gamma_\infty - 1) \tilde{T}_\infty \right). \quad (4)$$

Although subsonic and supersonic or even hypersonic boundary layers are similar in many respects, some notable differences also exist. Typically, incompressible flows are governed by the continuity and momentum equations alone. For compressible flows, also the energy equation and an equation of state for the gas must be considered. Hence, additional variables, such as the temperature and the density have to be taken into account when dealing with compressible flows, unlike for incompressible flows. Moreover, properties such as the viscosity or the thermal conductivity may be a function of these variables, and this function must be known. Also, internal energy of the gas depends on the pressure and temperature.

Investigations of hypersonic flow often use a so-called unit Reynolds number of $\tilde{Re}_{unit} = Re_\infty Ma_\infty / \tilde{L}_{ref}$ to describe freestream conditions. For a calorically perfect case in the freestream, the freestream pressure \tilde{p}_∞ correlates to the unit Reynolds number as follows:

$$\tilde{p}_\infty = \sqrt{\tilde{R}\tilde{T}_\infty\gamma_\infty^{-1}} \tilde{\mu}_\infty Re_\infty / \tilde{L}_{ref} = \sqrt{\tilde{R}\tilde{T}_\infty\gamma_\infty^{-1}} \tilde{\mu}_\infty Ma_\infty^{-1} \tilde{Re}_{unit}. \quad (5)$$

The same definitions that have been given here also apply to the notes for part II, Ref. [1].

1.1 Hypersonic High-Temperature Boundary-Layer Flows

In the boundary layer, the flow velocity changes from the freestream speed at some small distance from the wall down to zero at the no-slip wall. In this zone, kinetic energy is converted into internal energy. The temperature increases with internal energy, and hence the temperature in the boundary layer for a vehicle moving at hypersonic speeds can be an order of magnitude higher than in the freestream. The same argument applies to the temperature downstream of a bow shock. This may lead to so-called high-temperature gas effects, which may influence boundary-layer dynamics.

Due to high-temperature gas effects, the thermodynamic and transport properties, such as the gas specific heat and viscosity, are a function of temperature, and eventually for even higher temperature may depend on both temperature and pressure as well as local gas composition owing to chemical dissociation reactions and barodiffusion in the gas mixture [2].

1.1.1 High-Temperature Gas Effects

In order to illustrate the effect of temperature on gas properties, let us first consider a gas at rest. In the absence of any high-temperature gas effects, the gas commonly behaves as a calorically perfect gas. This is still true at moderately high temperature for a gas of a single species. In this case, its internal energy is proportional to the temperature and hence its specific heat is constant. In most practical applications, the fluid is a mixture of gases, for example air composed of atomic and diatomic species. At low temperature, vibrational and electronic modes

of the molecules are not excited and the gas mixture still behaves as a calorically perfect gas. As temperature increases, these modes get excited and the internal energy is a non-linear function of a single temperature due to the excitation of vibrational and electronic modes of the molecules. For a gas composed of one or more molecular species, also the specific heat becomes a function of temperature. If thermal-relaxation characteristic time scales are very small, such a gas is in thermal equilibrium and called a thermally perfect gas. Properties of a thermally perfect gas depend only on the (single) temperature. A gas in thermal non-equilibrium is described by multiple temperatures, but this situation is beyond the scope here.

If the temperature remains below a certain threshold, chemical reaction rates are low and the composition of the gas mixture does not change. For higher temperature, however, chemical reactions may cause the molecules to dissociate and hence change the composition of the mixture. If there is no flow, the dissociating gas is in local thermodynamic equilibrium everywhere after some time. For a gas in equilibrium, its composition is computed from two variables describing the thermodynamic state, such as pressure and temperature or density and internal energy.

For a gas moving at high speed, we need to take into account the characteristic time scales based on the mass flow rate in addition to all chemical reaction and thermal relaxation characteristic time scales. Three distinct regimes are typically distinguished, based on a comparison of the characteristic flow time scale with all chemical-reaction and thermal-relaxation characteristic time scales. This relation is typically expressed by one or more *Damköhler numbers* Da .

If the Damköhler number is large ($Da \rightarrow \infty$), chemical reaction rates are much larger compared to the convective mass transport rate, and the dissociating gas is in local thermodynamic equilibrium. In equilibrium, the moving gas' composition depends, again, on only two thermodynamic quantities provided that the elemental composition is constant.

If this number is very small ($Da \rightarrow 0$), the residence time of the fluid is much smaller than the chemical reaction time or thermal relaxation time and hence the flow is in a frozen state, i.e. the gas composition will remain fixed and does not change composition due to reactive process. For such a frozen gas mixture of atoms and molecules, the specific heat increases with temperature due to the excitation of vibrational modes.

If the Damköhler number is finite, the gas is said to be in chemical non-equilibrium or in a state of finite-rate chemical reactions, and its composition is governed by transport equations for the chemical species densities. Hence, the regime of finite-rate chemistry, or non-equilibrium chemistry, lies in between the two limiting states $Da \rightarrow 0$ and $Da \rightarrow \infty$. For reacting flow with dissociation, the gas mixture will change downstream in the boundary layer, and with it all thermodynamic gas properties as well as the evolution of the boundary layer itself.

The chemical reaction rate depends on a number of factors, such as the pressure and gas composition, but its dependence on temperature is most important for the type of high Mach number boundary-layer flows considered here. If the freestream temperature is not very high and the flow field is effectively frozen, the gas composition may still change due to diffusion if strong concentration gradients are present. However, diffusion coefficients are typically small so that this process is unlikely to be important for the dynamics of the flow.

Finally, the surface can also influence the gas composition due to catalytic effects. The details of these effects are neglected here, i.e. we consider only non-catalytic surfaces. The elemental mole fractions are assumed to be constant in the flow.

In the literature on hypersonic flow, a number of different expressions are used to describe the presence of high-temperature gas effects. Corresponding expressions include 'finite-rate chemistry', 'non-equilibrium chemistry' or 'real gas effects'.

1.1.2 Vehicle Configurations

The way high temperature gas effects influence boundary-layer dynamics may vary with the type of vehicle and its mission. For slender bodies at hypersonic speeds, the temperature at the boundary-layer edge may be comparable to the temperature of the environment through which the vehicle moves, owing to the small deflection angle of the shock at the leading edge of the vehicle. For these conditions, the temperature inside the boundary layer may be very high owing to a conversion of kinetic energy into thermal energy as explained above.

For blunt planetary (re-)entry vehicles, however, a strong increase in temperature is expected in the shock layer as a result of the severe bow shock in front of the vehicle. Hence, it is the boundary-layer edge temperature that may be highest in this case, for an example see figure 4 in Ref. [3]. For any of these cases the boundary layer could be in thermo-chemical equilibrium, chemical non-equilibrium and thermal equilibrium, or even in full thermo-chemical non-equilibrium including gas-surface interaction.

1.1.3 Numerical Methods for Flows with High-Temperature Gas Effects

Refs. [4, 5] distinguish between two general approaches to handle high-temperature gas effects within numerical simulations. The first one is the direct method, in which the flow computation is performed simultaneously with the solution of an additional set of explicit or implicit equations to obtain the thermodynamic and transport properties of interest. The corresponding additional equations may be derived from first principles assuming a certain atomic/molecular model [for an example based on a rigid-rotator and harmonic-oscillator model see Ref. 6]. The direct method typically requires only a few empiric model constants, and it can be applied for any Damköhler number.

The second general approach relies on a pre-computation of thermodynamic and transport properties, for which the mentioned first-principles method is run in a pre-processing step prior to the flow computation. This second approach can be denoted as indirect method and it can further be divided into two subgroups, depending on whether interpolation or curve-fitting techniques are used to extract actual quantities from pre-computed values. This second approach can only be used for the simulation of flows in local thermodynamic equilibrium, i.e. for $Da \rightarrow \infty$ and thermally perfect gas. However, it is computationally much less expensive compared to the direct method.

Numerical methods for finite-rate chemistry are routinely used for time-dependent flows with combustion [7–11]. The combustion community typically uses the expressions ‘detailed chemistry’ or ‘complete chemical scheme’ in order to describe their approaches. Most methods for combustion rely on a low Mach number formulation, and hence they are not applicable to the hypersonic flow regime.

A number of numerical methods capable of handling the high-temperature regime including finite-rate chemistry have been reported in which an unsteady solution to the compressible Navier-Stokes equations at hypersonic speeds has been sought [12–17]. The complexity associated with the combination of unsteady boundary-layer instability waves that cause transition, high Mach numbers, and high temperatures makes such time-dependent simulations challenging.

1.2 Introduction to Laminar-Turbulent Transition

Two distinct states of a boundary layer exist: the laminar and the turbulent state. The change from the laminar to the turbulent state is called laminar-turbulent transition. Hydrodynamic instability is a central cause of the breakdown to a turbulent flow for incompressible as well as for compressible flows. Both linear and nonlinear instabilities are key ingredients in the transition process. For hypersonic chemically reacting boundary layers,

transition phenomena are not well understood even for simple cases, although progress has been made in recent years. Ref. [18] contends that correlation-based methods [19] for transition prediction widely used by vehicle designers are not reliable and might at best be useful for re-entry vehicles only. He further argues that these methods should be replaced by linear stability theory [20], but the latter methods suffers from deficiencies due to non-parallel effects as explained below.

1.2.1 Laminar and Turbulent Boundary Layers

The laminar boundary-layer state corresponds to a stratified flow with no fluid exchange taking place between each quasi wall-parallel layer and the flow is in a steady state. In contrast, the turbulent state is characterized by a strong mixing of mass, momentum, and energy. Furthermore, the turbulent flow field is highly fluctuating due to a chaotic, random motion in conjunction with coherent flow structures. In turbulent flows the wall-normal momentum and kinetic as well as thermal energy exchange is larger than in laminar flows.

Turbulent flow possesses a larger velocity gradient at the wall resulting in higher skin friction. For high-speed compressible flow, turbulent flow also leads to a significant increase in temperature on or near the surface due to mixing. Turbulent flow may therefore be undesirable for the surface of hypersonic vehicles due to the high heat load experienced by the thermal protection system [2]. On the other hand, turbulence may be desirable for the inlet section of scramjets [21], as the presence of turbulence ensures proper fuel mixing within the combustor. The prediction of the transition location is a key factor in designing the thermal protection system.

1.2.2 The Three Stages of the Transition Process

The laminar-turbulent transition process will typically involve at least three stages independent of the type of breakdown: the receptivity stage, the stage of linear disturbance evolution and the stage of non-linear breakdown to turbulence.

During the receptivity process, external perturbations are converted into boundary layer disturbances. Typically, these external perturbations need to possess an appropriate length scale, e.g. a length scale comparable to the boundary-layer thickness, and/or frequency in order to efficiently penetrate the boundary layer. The receptivity process is treated in detail in Refs. [22, 23], and it will not further be considered here.

Once a set of small-amplitude perturbations is present in the boundary layer, they often get amplified due to a linear process, which can be of modal [24, 25] or non-modal [26] nature. Non-modal instability has not yet been investigated in detail for hypersonic boundary layers and will not be further considered here.

For a parallel flow, modal growth is usually unbounded (in time or space) and is called a primary instability. During modal primary instability exponential growth occurs. A selection of primary instability mechanisms is treated in § 1.3.

At the end of the linear growth stage, the flow field typically contains a certain form of coherent structure. This coherent structure can be a large-amplitude high-frequency wave, which travels in the main flow direction, or it can be a low-frequency streak, which introduces waviness in the direction normal to the main flow direction parallel to the wall. The large-amplitude modulation of the laminar base flow leads to a new instability. Depending on the type of primary perturbation, one can distinguish between wave breakdown and streak breakdown. Streak breakdown typically occurs as a result of non-modal instability, and as this instability has not yet been fully considered for hypersonic flows, the same is true for streak breakdown. Therefore, the discussion of the stage of non-linear breakdown in Ref. [1] will be restricted to wave breakdown.

Wave breakdown to turbulence is initiated when the primary flow structure, i.e. the wave, reaches a sufficiently large amplitude to create a new, so-called secondary instability. This secondary instability takes the

form of a linear parametric instability of the boundary layer distorted by the finite-amplitude streamwise wave [27]. Both a subharmonic as well as a fundamental instability may be active in a system consisting of two waves.

Very often, this secondary instability is a key process in exciting additional dimensions of the flow field, leading to rapid growth of corresponding perturbations. For instance, in a boundary layer altered by a large-amplitude two-dimensional wave, secondary instability leads to the emergence of disturbances that possess a waviness in the spanwise (z -)direction [28], eventually causing so-called lambda vortices. Moreover, secondary instability may lead to the emergence of subharmonic perturbations, such as vortex pairing in shear layers [29] which can not be excited directly by the nonlinear terms of the Navier-Stokes equations. The so-called oblique breakdown is a special case, where a pair of oblique waves induces streamwise streaks through non-linear interaction [30, 31]. This case can be regarded as a streak breakdown scenario, and it is hence not considered here.

At late stages of the breakdown process, the boundary layer gets filled with coherent vortical structures of decreasing scale. Additional processes that occur at this stage are localized instabilities [32] as well as vortical interactions, such as the effect of hairpin vortices on near-wall structures through induction and generation of pressure gradients along the wall. Shocklets may also occur in very high-speed flows.

1.2.3 Transition in Hypersonic High-Temperature Boundary Layers

The effect of high temperature on hypersonic boundary-layer instability has not been unraveled. Instead, evidence for a transition delay as well as enhancement exists. This contradiction may be attributed to the large number of governing parameters, such as reaction rates, as well as physical effects involved. In their § 5.4, Ref. [23] provide an overview of theoretical and numerical investigations of linear small-amplitude perturbations in hypersonic chemically reacting boundary layers.

Laminar-turbulent transition for flows of a high-temperature gas has been considered experimentally in Refs. [33, 34]. Theoretical approaches based on linearization have also been applied, using the parallel-flow assumption [35–41] or considering non-parallel flow [42] such as the parabolized stability equations (PSE)[39, 43]. Ref. [38] found that while chemical reactions destabilize the base flow, dissociation reactions diminish the growth of perturbations for a fixed base flow. Any theoretical calculation must either use a self-similar boundary layer or be preceded by a numerical simulation in order to obtain a steady-state boundary-layer flow, which is then used as a base flow in the theoretical approach. A number of numerical methods exist for this purpose [see for instance Refs. 44, 45]. While theoretical approaches provide valuable insight into the flow dynamics, the quantitative effects of the assumptions of linearity and parallel flow often used in theories need to be understood. In addition to experiments and theoretical investigations, unsteady numerical simulations can also be performed. Ref. [46] reports results of numerical simulations of boundary-layer instability waves for non-equilibrium conditions, considering the binary mixture of atomic and molecular oxygen. Ref. [47] investigates the receptivity and amplification of small boundary-layer perturbations for non-equilibrium air. Ref. [48] investigates the stability of boundary layers in local thermodynamic equilibrium, whereas Refs. [49, 50] consider flows with finite-rate chemical reactions.

Unfortunately, none of the methods based on the unsteady, non-linear Navier-Stokes equations, i.e., methods for the direct numerical simulation, have been validated against experiments. Hence, it has not yet been demonstrated that numerical simulation and experiments can accurately capture the growth rates of linear instability waves for chemically reacting high-speed flow. The validity of any numerical methods for the simulation of boundary-layer instability waves remains to be established. This is true for both equilibrium as well as non-equilibrium conditions.

Simulations of non-equilibrium conditions presently also suffer from a lack of established chemical models for non-equilibrium flow. For instance, Ref. [41] concludes that “the differences for linear stability growth rate prediction between . . . two [different] chemistry models for a Mach 10 boundary layer are larger than the differences between thermal nonequilibrium, chemical nonequilibrium, and chemical equilibrium.” A central problem is the uncertainty in chemical reaction rate coefficients of today’s models.

The strong bow shock in front of a hypersonic body with blunt nose can lead to the development of an entropy layer, which may host instability waves. A discussion of this entropy-layer instability in hypersonic flow can be found in § 8 of Ref. [23].

1.3 Introduction to Linear Boundary-Layer Instability

Linear instability denotes the amplification of initially small-amplitude perturbations in the boundary layer. As stated above, this process can be modal or non-modal. In case of modal instability, for boundary layers disturbances usually grow exponentially in the streamwise direction. This process will be treated in detail in § 3.0 below. Algebraic growth typically occurs for non-modal instability. The latter case is often denoted as transient growth, since disturbance growth is not unbounded even under the assumption of parallel flow. Non-modal or transient growth mechanisms may play a role for the transition process on blunt bodies in high-speed flow [51]. These mechanisms have been studied for compressible and supersonic flow [52–54], but will not be further considered here, as we focus on flat plates with sharp leading edges.

1.3.1 Linear Stability Theory and Eigenvalue spectra

An important tool for the investigation of model instability is linear stability theory, which will be treated only very briefly below. A detailed treatment of linear stability theory is given in Ref. [25].

Linear stability theory relies on several assumptions. In addition to the linearization around a given base flow, this base flow is assumed to be parallel. Hence, for boundary layers only the (mean) streamwise velocity profile $U = U_1$ as well as the temperature profile T are used as an input.

A normal-mode ansatz (complex eigenvalue: $\alpha = \alpha_r + i\alpha_i$, real frequency ω , real spanwise wave number β):

$$s' = \hat{s} \exp(i(\alpha x - \omega t + \beta z)), \quad (6)$$

is inserted into the linearized equations, which, for a calorically perfect gas, yields a solution vector of the form:

$$\hat{s} = [\hat{u}, \hat{v}, \hat{w}, \hat{p}, \hat{T}]^T. \quad (7)$$

In this equation, the streamwise velocity component is given by u , whereas wall-normal and spanwise velocity components are v and w , respectively. The pressure is given by p and the temperature by T .

The frequency ω can be calculated based on a fundamental wavenumber ω_0 via the relation $\omega = h\omega_0$, with a frequency coefficient h . Similarly, the spanwise wavenumber γ can be calculated from $\gamma = k\gamma_0$, with fundamental wave number γ_0 and spanwise wave number coefficient k . This allows to refer to a single oblique wave by specifying the pair of coefficients, i.e. (h, k) . In this nomenclature, a two-dimensional wave is given by $(h, 0)$.

The linearized equations are supplemented by homogeneous boundary conditions, which result in an eigenvalue problem [55]. A vanishing temperature disturbance is commonly assumed at the wall, corresponding to an isothermal condition for the disturbance. Such an assumption is typically even made if the base flow has been obtained with an adiabatic wall condition. The solution to the stability equation(s) is given by a combination of continuous and discrete eigenmodes, i.e. we deal with spectra of modes.

Two discrete eigenmodes are of particular interest in a supersonic boundary layer, commonly denoted as mode F and mode S [56]. A fast acoustic mode with a phase velocity of $c_{ph} = 1 + 1/Ma_\infty$ at the leading edge of the flat plate evolves into mode F further downstream. Analogously, mode S originates from a slow acoustic mode with a phase velocity of $c_{ph} = 1 - 1/Ma_\infty$ at the leading edge. Depending on Mach number and boundary conditions, only one of the two modes may exhibit two regions of disturbance growth, in which the amplification rate α_i is positive, or both modes may feature a single region of disturbance growth [56–58]. For compressible flow, multiple continuous spectra arise from the presence of acoustics, vorticity, and entropy modes. These continuous spectra are associated with non-model growth and are hence not considered here.

1.3.2 Non-Parallel Effects

In the theoretical treatment of boundary-layer instabilities, the growth of the boundary layer is usually assumed to be negligible, and the base flow is assumed to be only a function of the wall-normal direction, i.e. $U_{baseflow} = U(y)$ and $T_{baseflow} = T(y)$. This is called the parallel flow assumption.

For incompressible flow, non-parallel effects are surprisingly weak, and even for low-speed separated flows an almost perfect agreement between results based on linear stability theory (with parallel-flow assumption) and direct numerical simulations has been found, see for example Ref. [59]. For compressible flow, non-parallel effects are more pronounced. In particular, the growth rate as computed from various flow quantities (velocity components, wall pressure, etc.) may differ significantly, see for instance figure 9 in Ref. [60]. Differences between linear stability theory and the growth of disturbance wall pressure as observed in numerical simulations are particularly large, see figure 3 in [61].

Non-parallel effects can be considered in theoretical studies by using a different set of equations, the so-called parabolized stability equations. An overview of such investigations is given in Ref. [62], and an example for the application of these equations to hypersonic flow is given in Ref. [39].

1.3.3 Instability of Traveling Waves

The amplification of waves convected in the boundary layer may occur due to a number of instability mechanisms. For supersonic flow at a sufficiently high Mach number, viscous instability, inflectional instability and acoustic instability are the most important mechanisms. They all belong to the class of modal instabilities. It should be noted that the list of instabilities treated below is not exhaustive.

1.3.3.1 Viscous Instability

Investigations based on linear stability theory show that viscosity can be destabilizing for finite Reynolds numbers and moderately large Mach numbers. Such an effect of viscosity was predicted for an incompressible boundary layer [63, 64], and the corresponding amplification mechanism is called Tollmien-Schlichting(T-S) instability. For a boundary layer, exponential disturbance growth in streamwise direction is observed.

The main mechanism of this instability is a change of the phase relation between the wall-normal $v'=u_2$ and the streamwise $u'=u_1$ disturbance velocity component (for a two-dimensional wave) in the presence of a mean shear flow $\partial U/\partial y = \partial U_1/\partial x_2$, as it can be understood considering the Reynolds-Orr equation [see 65]. The first experimental evidence of the existence of this instability is attributed to reports in Ref. [66].

Three essential effects of compressibility should be noted. First, unlike for incompressible flow, oblique waves are usually more amplified. Second, viscous instability may not be as important for transition, and inflectional instability takes over instead. Finally, the temperature boundary layer (and hence the wall-temperature condition) plays an important role for compressible flow, as this boundary layer changes the viscosity, which

is temperature dependent, and hence also the shape and thickness of the momentum boundary layer. A typical example for this effect is the reduced boundary layer thickness for supersonic flows with wall cooling. In turn, this influences the amplification of disturbances, see for instance Ref. [48].

1.3.3.2 Inflectional Instability

At higher Mach numbers the effect of viscosity is only stabilizing, and often an inviscid inflectional instability picks up and becomes dominant.

According to the inflection-point theorem [67, 68], streamwise velocity profiles of boundary layers for incompressible flow that possess an inflection point away from the wall at $x_{2,s}$ are inviscidly unstable:

$$\left. \frac{\partial^2 U_1}{\partial x_2^2} \right|_{x_2=x_{2,s}} = 0. \quad (8)$$

In this equation, U_1 is the mean flow in the streamwise direction x_1 and x_2 corresponds to the wall-normal direction. For free shear layers, this inviscid inflectional instability is called a Kelvin-Helmholtz instability [29]. Citing an earlier report [69], Ref. [70] points out that the inflection-point criterion for inviscid instability for compressible flow is replaced by a criterion for the so-called generalized inflection point at $x_{2,s}$:

$$\left. \frac{\partial}{\partial x_2} \left(\rho \frac{\partial U_1}{\partial x_2} \right) \right|_{x_2=x_{2,s}} = 0. \quad (9)$$

In this equation, ρ corresponds to the density, U_1 is the mean flow in the streamwise direction x_1 and x_2 is the wall-normal direction. Such a generalized inflection point exists in insulated-wall flat-plate compressible boundary layers. This instability will be called Lees-Lin (L-L) instability below. Cooled-wall boundary layers may possess more than one generalized inflection point. In the literature, T-S and L-L instability waves are often called first-mode instability waves.

1.3.3.3 Acoustic Instability

For supersonic flows at a sufficiently high Mach number, it has been found that a family of trapped acoustic waves exist [55, 71]. Ref. [56] explains that a region of supersonic mean flow relative to the disturbance phase velocity is present and that the boundary layer behaves as an acoustic waveguide. Within this waveguide, acoustic rays are reflected by the wall and turn around near the sonic line as illustrated in figure 2 of Ref. [56]. This inviscid instability of acoustic nature is often called Mack, Mack-mode, or second-mode instability. At very high Mach numbers, the transition process is most likely driven by acoustic instability.

1.3.4 Parametric Effects

In the following, only a brief overview of parametric effects is given. For compressible flow, further details are discussed in Refs. [20, 72].

1.3.4.1 Reynolds Number

The typical streamwise wave length of a Tollmien-Schlichting wave, Lees-Lin wave, as well as a Mack wave, in the boundary layer scales with the boundary-layer thickness, i.e. the disturbance frequency decreases with the thickening of the boundary layer. Since the T-S instability is driven by viscosity, the corresponding amplification rate eventually decreases with increasing Reynolds number. For the essentially inviscid instabilities (e.g.

Kelvin-Helmholtz, Lees-Lin, Mack) disturbance amplification increases with increasing Reynolds number, as the damping effect of viscosity diminishes.

1.3.4.2 Pressure Gradient

A favorable pressure (streamwise pressure drop) stabilizes the boundary layer, whereas an adverse pressure gradient (streamwise pressure rise) increases linear boundary-layer instability. This observation holds for both Tollmien-Schlichting instability [73, 74] and Lees-Lin instability [75, 76]. A favorable pressure gradient decreases Mack instability [20], whereas an adverse pressure gradient increases this instability, as can be seen for instance for the separated supersonic flow in front of a two-dimensional roughness element [75, 76] or for a shock impinging the boundary layer [60].

1.3.4.3 Blowing/Suction at the Wall

Ref. [20] illustrates that the effect of wall suction is to stabilize the Mack instability for supersonic flow. For this type of flow, [77, 78] found that with increasing blowing rate, the amplification rate for Mack instability increases and moves to lower frequencies, while the phase velocity decreases.

Wall suction or favorable pressure gradient, i.e. anything that thins the boundary layer, causes the disturbance frequency to increase, since the instability wavelength scales with the boundary-layer thickness [35].

1.3.4.4 Heating/Cooling at the Wall

The boundary layer can be heated or cooled by means of changing the temperature at the wall. In this way, the thermal boundary layer changes, and with it the viscosity of the fluid as well as the speed of sound.

For compressible boundary layers, cooling destabilizes Mack instability waves, but stabilizes Tollmien-Schlichting waves. It also usually leads to an increase in typical disturbance frequency for Mack instability waves, since the corresponding wavelength (inversely proportional to the frequency) scales with the boundary-layer thickness [79], which is reduced by cooling. A comprehensive treatment of the effect of wall temperature for varying Mach number is given in Ref. [20].

1.3.4.5 Acoustic Coating

Ultrasonically absorptive coating may suppress Mack instability. This effect is only relevant for hypersonic flow, and further details can be found in § 6 of Ref. [56].

1.4 Scope

The present notes as well as Ref. [1] are only devoted to the discussion of hypersonic boundary layers with high-temperature gas effects. More precisely, we will only consider configurations in which the temperature at the boundary-layer edge situation is sufficiently low so that the gas in the freestream can be modeled as an calorically perfect gas, while the temperature inside the boundary layer may be very high. Configurations for which the opposite is true, i.e. high temperature in the freestream with wall cooling, are beyond the scope of these notes.

The reader should be familiar with at least some aspects of supersonic hydrodynamic instability theory as well as with hypersonic and high-temperature gas dynamics. An introduction to the latter field can be found in Ref. [2]. Supersonic hydrodynamic instability has seen rapid development in recent years, and comprehensive overviews can be found in Refs. [23, 56, 58].

case	Re_∞	Pr_∞	γ_∞	Ma_∞	\tilde{T}_∞ [K]	$\tilde{\rho}_\infty$ [kg m ⁻³]	\tilde{p}_∞ [Pa]	wall B.C.	references
A	10^4	0.69	1.397	10	350	$0.3565 \cdot 10^{-1}$	3596	$\partial T_w / \partial y = 0$	[35, 48–50]

Table 1: Freestream parameters for investigations of hypersonic boundary layer.

Below and in Ref. [1], we restrict ourselves to the discussion of basic physical effects with respect to linear and non-linear hydrodynamic stability, as they have been found from numerical simulations. Some of these effects, based on theoretical approaches as well as experiments, have been discussed in earlier lecture series, such as Refs. [45, 80]. Throughout these notes and in Ref. [1], we only consider fluids that are in thermal equilibrium. Therefore, any excitation of rotational and vibrational modes equilibrates infinitely fast, although it is noted that Ref. [81] found that thermal non-equilibrium may influence the laminar-turbulent transition process.

2.0 BASE FLOW

In case of laminar boundary-layer flow with only small-amplitude disturbances present, the time-averaged mean flow obtained from a numerical simulation can be considered a useful basis for the analysis of hydrodynamic stability. Therefore, such a flow is called a base flow. If a self-similar solution of the compressible boundary-layer equations exists, as it is the case for flow in local thermodynamic equilibrium as well as (often) for frozen flow, we can also consider this self-similar solution instead.

In order to illustrate the effect of chemical reactions on the mean flow, we will use a flat-plate boundary layer with adiabatic wall at a freestream Mach number $Ma_\infty = 10$. All results presented here have been obtained from numerical simulations [48–50]. In these simulations, the flow over a semi-infinite flat plate with a no-slip wall at $y = 0$ and a non-catalytic condition, i.e., $\partial \chi^s / \partial y|_{y_1} = 0$ with $\chi^s = \rho^s / \rho$, has been simulated (ρ^s is the partial density of species s and ρ is the density of the gas mixture). A fixed velocity is prescribed at the upper boundary $u_\infty = Ma_\infty$. The coordinate system is aligned with the plate, and its origin $[x, y]^T = [0, 0]^T$ is placed at the leading edge of the flat plate, with z corresponding to the spanwise direction. At the inflow location of the computational domain, which is placed downstream of the leading edge ($x_1 > 0$), a self-similar boundary-layer solution is prescribed.

The inflow location in the simulations was placed downstream of the leading edge in order to avoid having to deal with shocks in the leading-edge region. For the case of local thermodynamic equilibrium, the corresponding self-similar solution is prescribed at the inflow, whereas a self-similar condition for a frozen thermally perfect gas is prescribed otherwise. For non-equilibrium flows, a non-catalytic condition at the wall has been used for the species densities, i.e., $\partial \chi^s / \partial y = 0$. In all cases, the gas is five species air: $s = N, O, N_2, NO, O_2$. This test case is denoted as case A in table 1, with $Ec_\infty = 1$, and it has been previously considered for chemically reacting flow in equilibrium as well as non-equilibrium in Refs. [35, 48–50].

2.1 High-Temperature Gas Effects in a Flat-Plate Boundary Layer at Mach 10

Boundary-layer profiles for the streamwise velocity U/U_∞ and the temperature T/T_∞ at $Re_x = 2000$ are depicted in figure 1 for three different gas models: a frozen gas, five species air with finite-rate chemical reactions and five species air in local thermodynamic equilibrium. Both the results for local thermodynamic equilibrium and frozen flow based on the Navier-Stokes equations remain very close to the self-similar solution (not shown here, but see Ref. [49]). In the simulation, the equations solved for a frozen gas are identical to

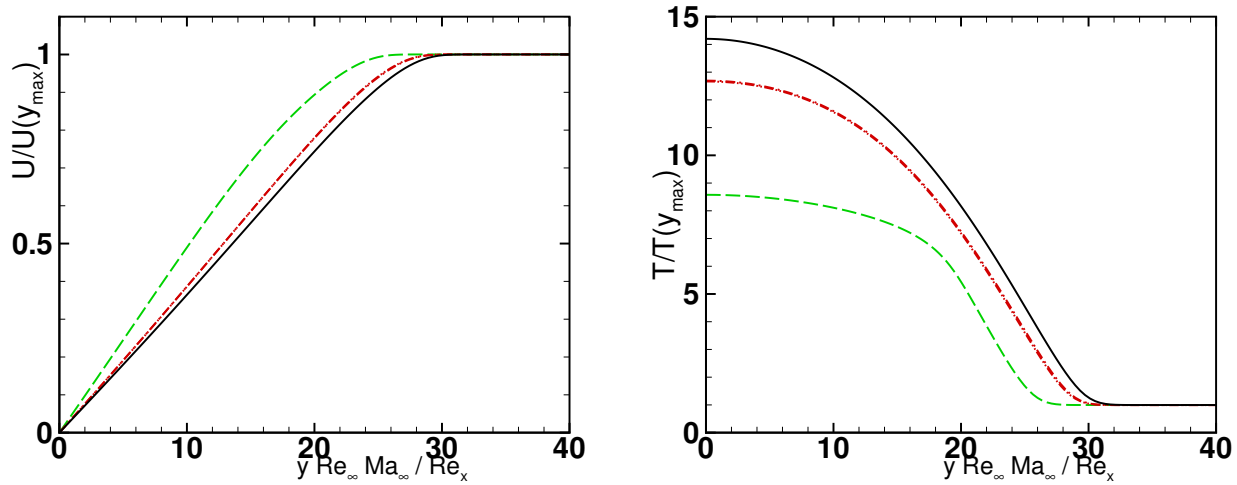


Figure 1: Boundary-layer profiles (left: U ; right: T) at $x = 40.0 / Re_x = 2000$, case A, for frozen air (solid line)[49], for finite-rate chemically reacting air in non-equilibrium (inflow at $x = 11.65$: dash-dotted line, and inflow at $x = 5.65$: dash-dot-dot line)[49], and for chemically reacting air in equilibrium (dashed line)[48].

those used for a finite-rate reacting gas, but reaction rates are set to zero in the former case.

By comparing the results obtained with different gas models, the effect of chemical reactions can be analyzed. Due to the adiabatic condition at the wall, the temperature is highest at the wall $y = 0$ (figure 1, right). This temperature is sufficiently high so that dissociation of molecular oxygen into atomic oxygen occurs for reactive models. A small amount of NO is also produced. The species mass fractions of atomic oxygen χ^O and χ^{NO} is hence largest at the wall and vanishes in the freestream, whereas χ^{O_2} decreases away from the wall towards the value present at the inflow $\chi^{O_2}(x_1)$, and which it reaches in the freestream [49].

The dissociation reactions are endothermic, and hence the temperature is lower in case of chemical reactions. The more of the molecular oxygen gets dissociated, the stronger the drop in temperature when compared with the frozen gas result. Hence, the case with finite-rate reactions exhibits only a moderate drop in wall temperature as it can be seen in the figure. The result for local thermodynamic equilibrium sees the largest drop in temperature close to the wall, as in this case the largest fraction of molecular oxygen has dissociated. At the streamwise location depicted, the wall temperature for the reacting case with finite-rate reactions has already dropped more than ten percent compared with the frozen gas, and it continues to decay slowly downstream.

The reduction of temperature close to the wall causes a reduction of viscosity in the wall-near region, as viscosity strongly depends on temperature. As a result, the velocity boundary layer is thinner in cases with chemical reactions, as it can be observed in figure 1 (left). In case of local thermodynamic equilibrium (dashed line in the figure), the shape of the velocity and temperature profiles are markedly different compared to the frozen and finite-reacting cases, in particular the temperature near the wall is almost constant up to half of the boundary-layer thickness, and the velocity profile is slightly fuller.

2.2 The Effect of Freestream Temperature

In order to illustrate the effect of freestream temperature, this temperature is slightly decreased from $\tilde{T} = 350$ K (case A) to $\tilde{T}_\infty = 278$ K. Such a setup with lower freestream temperature was investigated in Ref. [37], and more recently in Refs. [41, 49]. The physio-chemical model used in Refs. [41, 49] is very similar but differs slightly from the one applied in Ref. [37].

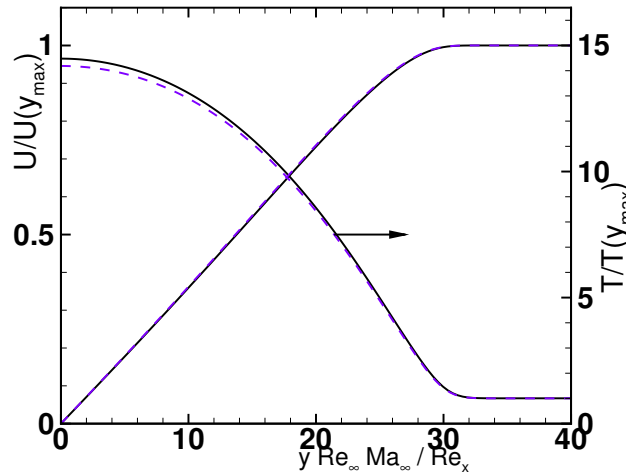


Figure 2: DNS results [49] for frozen air (solid line) and for finite-rate chemically reacting air (dashed line) for conditions similar to case A, but at a lower temperature ($\tilde{T}_\infty = 278K$).

For the case of the reduced freestream temperature, the boundary-layer profiles for finite-rate reactive flow are in very close agreement with those obtained for the corresponding frozen flow (figure 2). Hence, for the lower freestream temperature even the flow modeled as reactive flow essentially behaves as frozen. The only difference visible is a slightly lower wall temperature in the finite-rate case.

The Damköhler numbers, which relate the characteristic flow time scale with the chemical reaction time scales, may be used to explain this effect of freestream temperature. The non-dimensional species source term can be regarded as such a Damköhler number [49] for each species s , respectively, and its value along the wall is depicted in figure 3. For the case A with $\tilde{T} = 350$ K (figure 3, left), close to the inflow location at $x = 11.65$, the production of atomic oxygen is large and then decreases gradually downstream since the wall temperature decreases while the concentration of atomic oxygen continues to increase.

For the lower freestream temperature (figure 3, right), however, we see that all Damköhler numbers remain below 2×10^{-4} , indicating that the residence time of the fluid is much smaller than the chemical reaction time and hence the flow is effectively frozen. For the lower freestream temperature $\tilde{T}_\infty = 278$ K, the Damköhler number is roughly an order of magnitude smaller than that for the case with higher temperature $\tilde{T} = 350$ K (compare figure 3, left and right plots).

3.0 LINEAR DISTURBANCE EVOLUTION IN HYPERSONIC FLOW

In order to better understand the effect of chemical reactions on hydrodynamic instability, we will consider the same gas models as in the previous section. For compressible boundary layers, cooling destabilizes Mack instability waves, as it has been described in § 1.3.4. It also usually leads to an increase in typical disturbance frequency for Mack instability waves, since the corresponding wavelength (inversely proportional to the frequency) scales with the boundary-layer thickness [79].

In the last sections § 2.1 and 2.2, it has been described that the effects on the base flow caused by chemical reactions are very similar to those that occur due to cooling at the wall. Hence, it is expected that the effects of wall cooling and chemical reactions are similar also for linear disturbance evolution. It was also described above that in the case of local thermodynamic equilibrium, the shape of the velocity and temperature profiles are

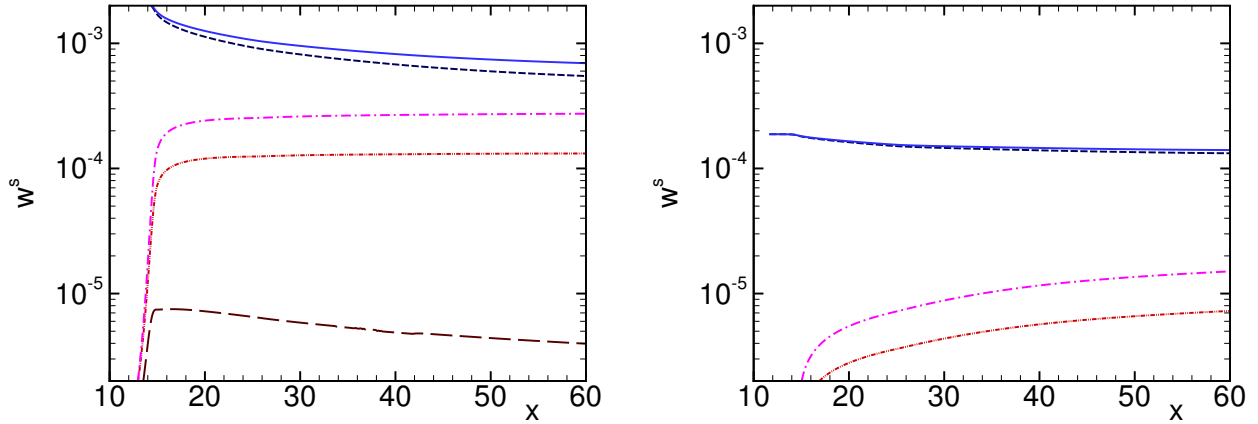


Figure 3: Non-dimensional species source term w^s at the wall from DNS [49] (from top to bottom: $s = O_2, O, NO, N_2, N$). Left: $\tilde{T}_\infty = 350$ K, right: $\tilde{T}_\infty = 278$ K.

markedly different compared to the frozen and finite-reacting cases, and hence the effects of chemical reactions in this case may not be reduced to just the effect of wall cooling. This conjecture will be checked in § 3.1.

As the freestream Mach number for the cases considered here is high, we will mainly focus on second mode / acoustic mode amplification. This is unlike Ref. [35], which performed a comparison between calorically perfect gas and reacting gas. In order to single out the effect of chemical reactions, a comparison between a finite-rate reacting and a frozen gas is performed here instead.

Numerical simulations offer the opportunity to verify certain conjectures by running the same conditions with different models, i.e. frozen versus reacting flow. In numerical simulations, typically one or more disturbances of a fixed non-dimensional frequency ω are forced via wall blowing/suction within a disturbance strip placed close to the inflow, respectively. The frequency is defined as (\tilde{f} is the dimensional frequency):

$$\omega = F Ma_\infty^2 Re_\infty, \text{ with } F = 2\pi \tilde{f} (\tilde{\mu} / (\tilde{\rho} \tilde{u}^2))_\infty. \quad (10)$$

The amplification rate α_i is computed from the wall-normal velocity component, taking the maximum in the wall-normal direction first:

$$\alpha_i(x) = \frac{1}{\hat{v}^{max}} \frac{\partial \hat{v}^{max}}{\partial x}. \quad (11)$$

The phase velocity c_{ph} is computed from the wall pressure ($p_w = p(y=0)$), with c_{ph} non-dimensionalized by the free-stream velocity, i.e. $c_{ph} = \tilde{c}_{ph} / \tilde{u}_\infty = \tilde{c}_{ph} / (\tilde{a}_\infty Ma_\infty)$:

$$c_{ph} = Re_\infty Ma_\infty F \left(\frac{\partial \Phi_p}{\partial x} \right)^{-1}. \quad (12)$$

In these equations, \hat{v} and Φ_p correspond to the amplitude and phase of the instability wave, respectively, that one can obtain from a double Fourier analysis in time and spanwise direction. Again, the definitions and equations given above also apply to the notes for part II, Ref. [1].

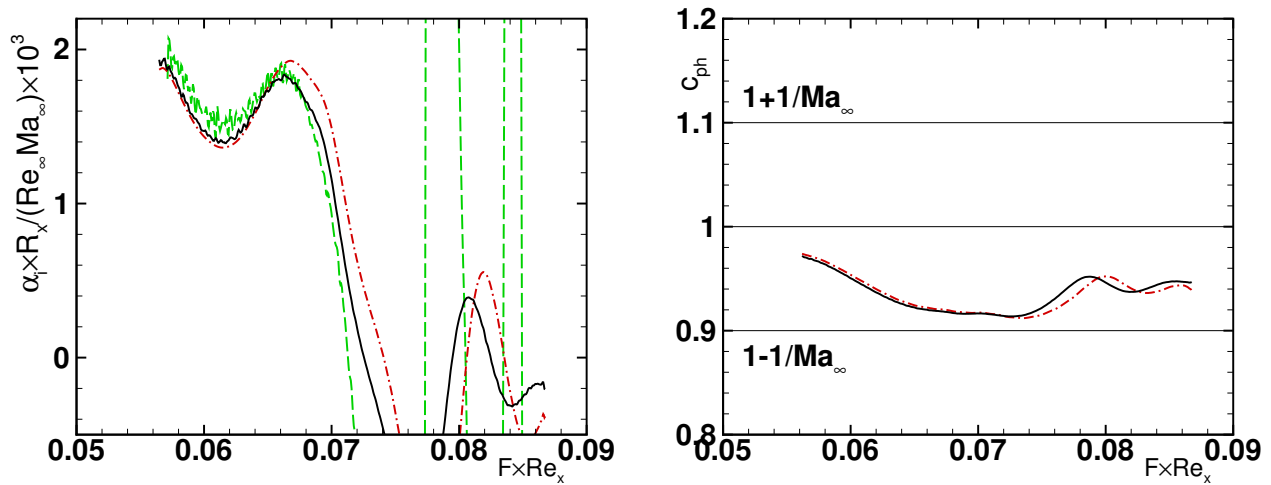


Figure 4: DNS results, case A, for frozen air (solid line)[49], for chemically reacting air in non-equilibrium (dash-dotted line)[49], and for chemical equilibrium (dashed line, only shown in the left figure)[48]. Results have been obtained for a fixed frequency parameter $F = 0.34 \times 10^{-4}$. Left: Amplification rate (computed from the wall-normal velocity component). Right: phase velocity for a disturbance wave (computed from the wall pressure).

3.1 High-Temperature Gas Effects in a Flat-Plate Boundary Layer at Mach 10

For the boundary-layer flows discussed in § 2.1 (case A), amplification rates and phase velocities are depicted in figure 4. Again, the same three different gas models have been considered: a frozen gas, five species air with finite-rate chemical reactions and five species air in local thermodynamic equilibrium. It has earlier been shown that these three cases also exhibit different mean flow profiles. In particular, it was found that the effect of chemical reactions here is broadly similar to cooling at the wall.

When comparing amplification rates between a frozen gas (solid line in figure 4, left) and the gas with finite-rate chemical reactions (dash-dotted line in figure 4, left), it can be observed that the effect of finite-rate chemical reactions is indeed consistent with those one would expect from wall cooling. In particular for higher frequencies (in the figure: $F \times Re_x > 0.066$), amplification rates are higher for the finite-rate reacting flow compared to the frozen flow. For a fixed \tilde{T}_∞ chemical reactions lead to a more unstable boundary layer, in agreement with observations of Ref. [38] using linear stability theory.

Moreover, amplification extends to higher values of $F \times Re_x$, i.e. the region of amplified frequencies or streamwise positions becomes larger. This is unlike for cooling at the wall, where one would expect to see mainly a shift of the instability region to higher values of $F \times Re_x$ instead, but it can be understood from the downstream evolution of the base flow profile. Due to ongoing reactions downstream, i.e. for increasing streamwise Reynolds numbers Re_x , the temperature at the wall continues to decrease downstream. This implies that the boundary layer can be viewed to be increasingly cooler close to the wall downstream, when compared with the corresponding frozen flow. As wall cooling leads to higher amplification, the amplification rate for the reacting flow is larger than that for the frozen flow at the same location, and this effect increases downstream. Another contributing effect may be the reduced growth of the boundary layer due to lower temperature and hence lower viscosity close to the wall. This suggests that the boundary layer grows less quickly with increasing streamwise Reynolds number, i.e. one could argue that the abscissa gets stretched compared to the frozen flow. A difference is hardly visible for the phase velocity (figure 4, right).

Interestingly, the amplification rate for flow in local thermodynamic equilibrium is the lowest of all conditions for $0.075 > F \times Re_x > 0.066$. Hence, although the boundary-layer profile for the finite-rate profile

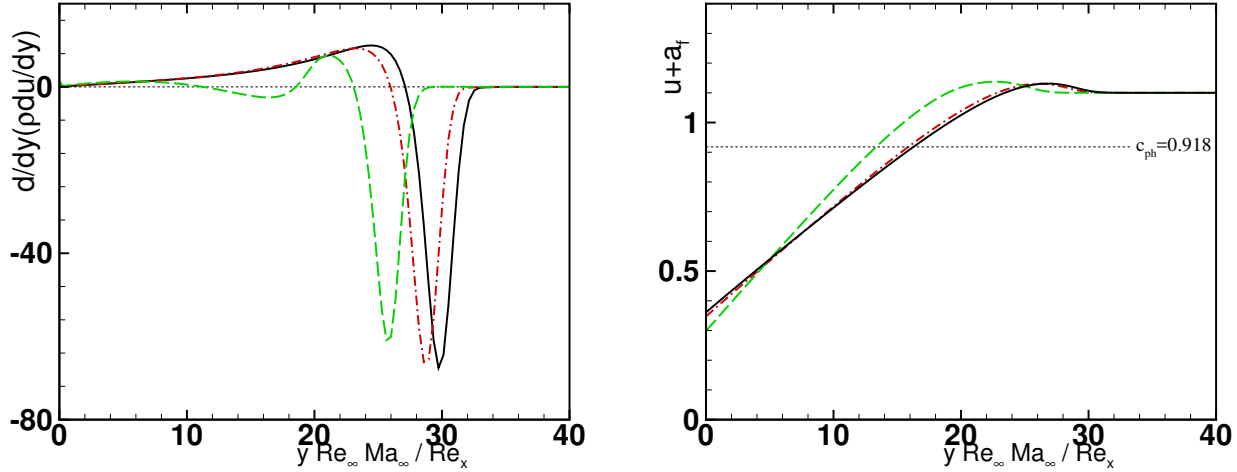


Figure 5: DNS results, case A, for frozen air (solid line)[49], for chemically reacting air in non-equilibrium (dash-dotted line)[49], and for chemical equilibrium (dashed line)[48]. Left: sum of the streamwise velocity and the local speed of sound $u + a_f$. Right: $d/dy(\rho du/dy)$ at $Re_x = 2000$.

lies in between those for frozen and for local thermodynamic equilibrium flow, the amplification rate is highest. This suggests that the analogy drawn between cooling at the wall and chemical reactions only works for small or moderately large deviations from a frozen state. For a strong deviation, as presented by a flow in local thermodynamic equilibrium, it was pointed out above that the shape of the boundary layer profiles changed significantly. This effect is likely to contribute also to a more complex change in instability. Ref. [35] also concluded that the effects of equilibrium chemistry is not entirely analogous to the effect of wall cooling.

In order to better understand the stability characteristics of the boundary layer for the different gas models, we now consider quantities known to influence both first-mode and second-mode instabilities. The wall-normal distance of the location where $u + a_f = c_{ph}$ influences the acoustic (Mack or second-mode) instability of a boundary layer, with the local speed of sound defined as $a_f = \sqrt{\gamma_f \bar{p} / \bar{\rho}} (\tilde{c}_{p,\infty} (\gamma_\infty - 1) \tilde{T}_\infty)^{-1}$. According to figure 4(right), we can assume that the phase speed of the disturbance is roughly $c_{ph} = 0.918$. Figure 5(right) shows that the wall-normal distance of the location where $u + a_f = c_{ph}$ does not differ much between the frozen and the non-equilibrium flow. Compared with the frozen flow, the non-equilibrium flow possesses a larger streamwise base velocity due to the thinner boundary layer. However, this is compensated by a smaller a_f due to the lower temperature. The competition of these two factors will govern the overall change in the instability of the base flow, which is hence not obvious, unlike in the case of the first-mode instability.

The presence and wall-normal distance of one or more generalized inflection points, fulfilling the condition $d/dy(\rho du/dy) = 0$, influences the inflectional (Lees-Lin or first-mode) instability of a boundary layer. This quantity is shown in figure 5(left). For the frozen flow, a generalized inflection point is located at $y Re_\infty Ma_\infty / Re_x = 27.1$, whereas it is located closer to the wall for the chemically reacting air in non-equilibrium ($y Re_\infty Ma_\infty / Re_x = 26.0$). It sits even closer to the wall for chemical equilibrium ($y Re_\infty Ma_\infty / Re_x = 23.1$, with another inflection point located at 11.3). This suggests that chemical reactions reduce the inflectional instability, which is in line with the observations of Ref. [35].

This can indeed be confirmed when considering oblique waves with large spanwise wave numbers k . We see in figure 6 that perturbations with small spanwise wave numbers ($|k| < 4$) continue to be unstable with respect to the Mack mechanism for larger values of $F \times Re_x$ compared to a frozen gas (compare the top three dashed and solid lines in figure 6), similar to what has just been observed for two-dimensional disturbances.

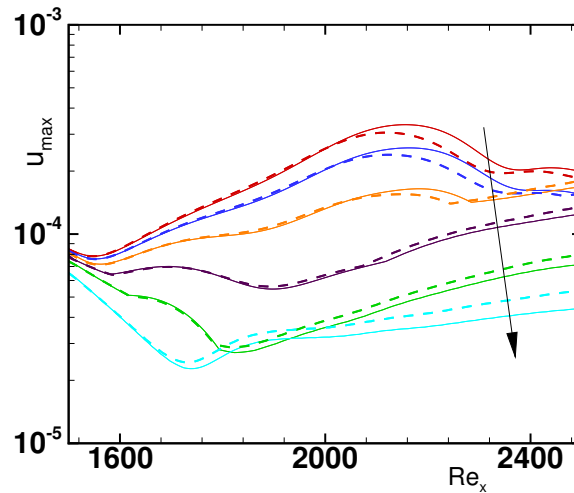


Figure 6: DNS results [50], case A, for a frozen gas (dashed lines) and a chemically reacting gas (solid lines). Small-amplitude linear results ($A_v^{(1,0)} = 0$, $A_v^{(1,\pm k)} = 10^{-4}$) for modes $(1, \pm k)$ with $k = 1 \dots 6$ (from top to bottom as indicated by the arrow).

The peak amplification rate for these perturbations is also slightly higher for the reacting gas than that for frozen gas. On the other hand, highly oblique ($k \geq 4$) first-mode waves are less amplified for the reacting gas (again, compare the respective dashed and solid lines in figure 6), which is consistent with the discussion of the location of the generalized inflection point above, suggesting that finite-rate chemical reactions stabilize first-mode instability waves. For moderately reactive flows such as case A here, the effect of chemical reactions is hence overall very similar to the effect of cooling at the wall.

3.2 The Effect of Freestream Temperature

The specific heat increases with temperature due to vibrational excitation, and hence increasing the freestream temperature from $\tilde{T}_\infty = 350 K$ to $425 K$ causes the non-dimensional wall temperature to decrease from $T_{wall} = 14.22$ to 13.98 even for the frozen gas. For a flow with finite-rate chemical reactions, an even stronger reduction of the wall temperature may occur depending on the streamwise location, for instance from $T_{wall} = 12.6$ to 11.7 at $Re_x = 2122$. As stated above, this effect of a reduction of non-dimensional wall temperature induced by the temperature-dependent gas properties is effectively analogous to cooling at the wall, which is known to increase the Mack-type amplification.

Such an increase in amplification rate with increasing freestream temperature can indeed be seen for both the frozen gas and for the reacting gas (figure 7, left). For the reacting gas, this effect is most pronounced at higher values of $F \times Re_x$, whereas at lower values the stability remains almost unchanged.

If we lower the temperature from $\tilde{T}_\infty = 350 K$ to $278 K$, we found in § 2.2 that the Damköhler numbers become so small that the flow becomes frozen. We can verify this conjecture by comparing results from a simulation in which reactions have been deliberately suppressed, i.e. flow modeled as frozen, with those for which finite-rate reactions may occur according to the gas model applied, with the reaction rate determined by the conditions in the boundary layer. The amplification rate α_i of an instability wave for such a boundary layer (with $\tilde{T}_\infty = 278 K$) is depicted in figure 7 (right). This figure confirms that the difference between results for a frozen gas and a finite-rate reacting gas is indeed very small. Comparing the amplification rate in this figure with those in figure 7 (left), we can see that the amplification is reduced as a result of decreased freestream

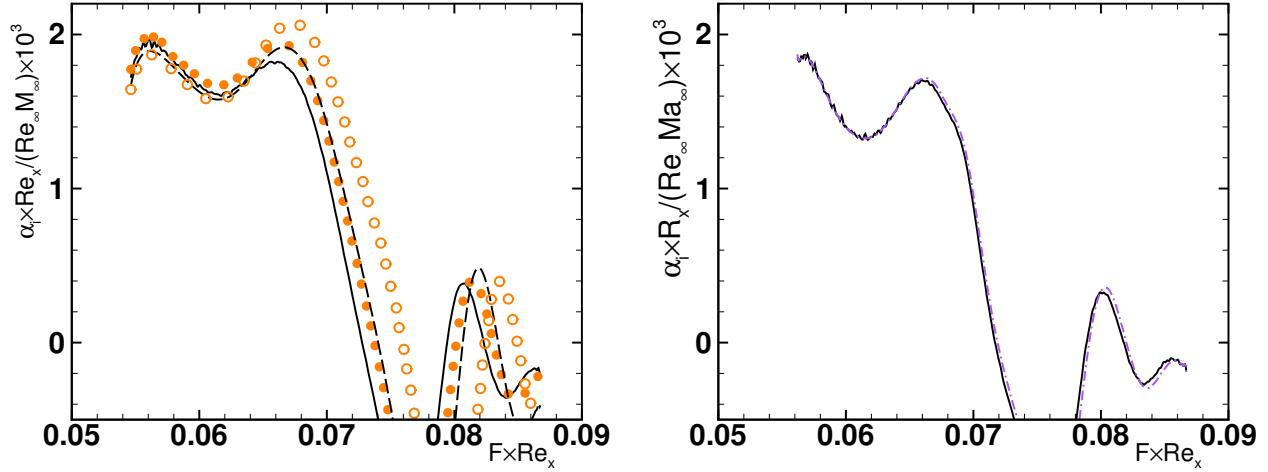


Figure 7: Amplification rate $\alpha_i(x) = 1/\hat{v}_{max} \partial \hat{v}_{max} / \partial x$ of small-amplitude mode (1, 0) from DNS. Left: Results for two different freestream temperatures : $\tilde{T}_\infty = 350\text{ K}$ (lines) and $\tilde{T}_\infty = 425\text{ K}$ (symbols)[50] for frozen air (solid line,●) and chemically reacting air (dashed line,○). Right: Results for a freestream temperature $\tilde{T}_\infty = 278\text{ K}$ [49] for frozen air (solid line) and for finite-rate chemically reacting air (dash-dotted line). Results have been obtained for a fixed frequency parameter $F = 0.34 \times 10^{-4}$.

temperature \tilde{T}_∞ , as expected.

The effect of the temperature boundary condition at the wall for the disturbance can be investigated by comparing simulation results for an adiabatic disturbance boundary condition with those obtained for an isothermal condition, while the boundary condition for the base flow remains adiabatic. The isothermal disturbance condition has been used for all results presented above. For a gas in chemical equilibrium [48] as well as for a frozen gas [49], the amplification for an isothermal boundary condition is slightly lower than that for an adiabatic condition, but differences are small. The same observation holds for a calorically perfect gas [75, 82].

3.3 Comparison between DNS and Linear Stability Theory

DNS results for the isothermal perturbation condition are compared with the results from linear stability theory in figure 8. The theoretical results are taken from figure 5 of Ref. [41]. Amplification rates from DNS compare favorably with those from linear stability theory, although such an agreement is certainly not perfect. Any differences may be due to the parallel-flow assumption applied in the theory, but such a conjecture needs to be verified in the future.

Figure 9 depicts amplitude and phase functions for the case of finite-rate chemistry. Qualitatively, velocity, temperature and density profiles do not differ strongly between a gas in thermodynamic equilibrium and a finite-rate chemically reacting gas. The main difference is a fuller profile of the temperature amplitude function in the finite-rate case compared to the respective amplitude functions in equilibrium, given in Ref. [48] (their figures 19 and 20), as well as larger temperature amplitudes close to the wall. For equilibrium conditions, Ref. [48] found that differences for amplitude and phase functions between DNS and LST are small.

ACKNOWLEDGMENTS

The author would like to thank Thierry Magin, von Karman Institute for Fluid Dynamics, Gianluca Iaccarino, Stanford University, and Eric Shaqfeh, Stanford University, for their contributions and collaboration that lead to

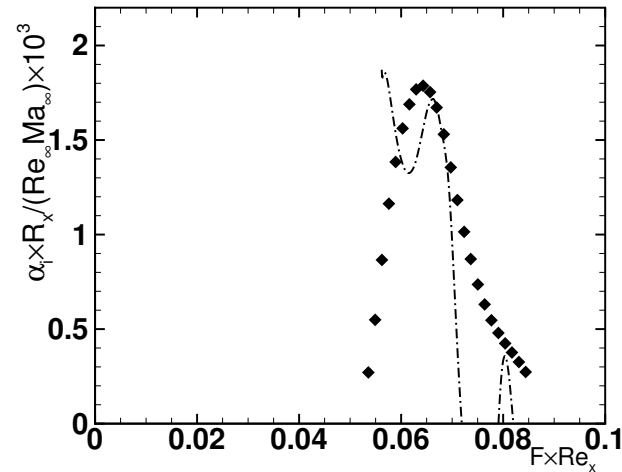


Figure 8: Amplification rate for a freestream temperature $\tilde{T}_\infty = 278 \text{ K}$ [49] for frozen air from DNS [49] (dash-dotted line), compared with the results of linear stability theory (symbols), the latter taken from figure 5 of Ref. [41]. DNS results have been obtained for a fixed frequency parameter $F = 0.34 \times 10^{-4}$, whereas linear stability theory results have been obtained for a fixed streamwise Reynolds number $Re_x = 1982.4$.

the research results presented in this manuscript. The author would also like to thank Fabio Pinna, von Karman Institute for Fluid Dynamics, for comments on this manuscript.

REFERENCES

- [1] Marxen, O., “Hydrodynamic Stability of Hypersonic Chemically-Reacting Boundary Layers II,” *STO-AVT-289 - Multiphysics phenomena analysis on boundary layer stability in hypersonic regime*, VKI lecture series, 2017.
- [2] Anderson, J. D., *Hypersonic and High Temperature Gas Dynamics*, AIAA, 2000.
- [3] Johnson, H. B. and Candler, G. V., “Orbiter Boundary Layer Stability Analysis at Flight Entry Conditions,” *AIAA Paper*, Vol. 2010–457, 2010.
- [4] Srinivasan, S., Tannehill, J. C., and Weilmuenster, K. J., “Simplified curve fits for the thermodynamic properties of equilibrium air,” Tech. Rep. L-16276, NAS 1.61:1181, NASA-RP-1181, Langley Research Center, NASA, 1987.
- [5] Srinivasan, S. and Tannehill, J. C., “Simplified curve fits for the transport properties of equilibrium air,” Tech. Rep. ISU-ERI-AMES-88405, NAS 1.26:178411, NASA-CR-178411, NASA, 1987.
- [6] Chalot, F. and Hughes, T. J. R., “A consistent equilibrium chemistry algorithm for hypersonic flows,” *Computer Methods in Applied Mechanics and Engineering*, Vol. 112, No. 1-4, 1994, pp. 25 – 40.
- [7] Najm, H. N., Wyckoff, P. S., and Knio, O. M., “A Semi-implicit Numerical Scheme for Reacting Flow. I. Stiff Chemistry,” *J. Comput. Phys.*, Vol. 143, 1998, pp. 381–402.

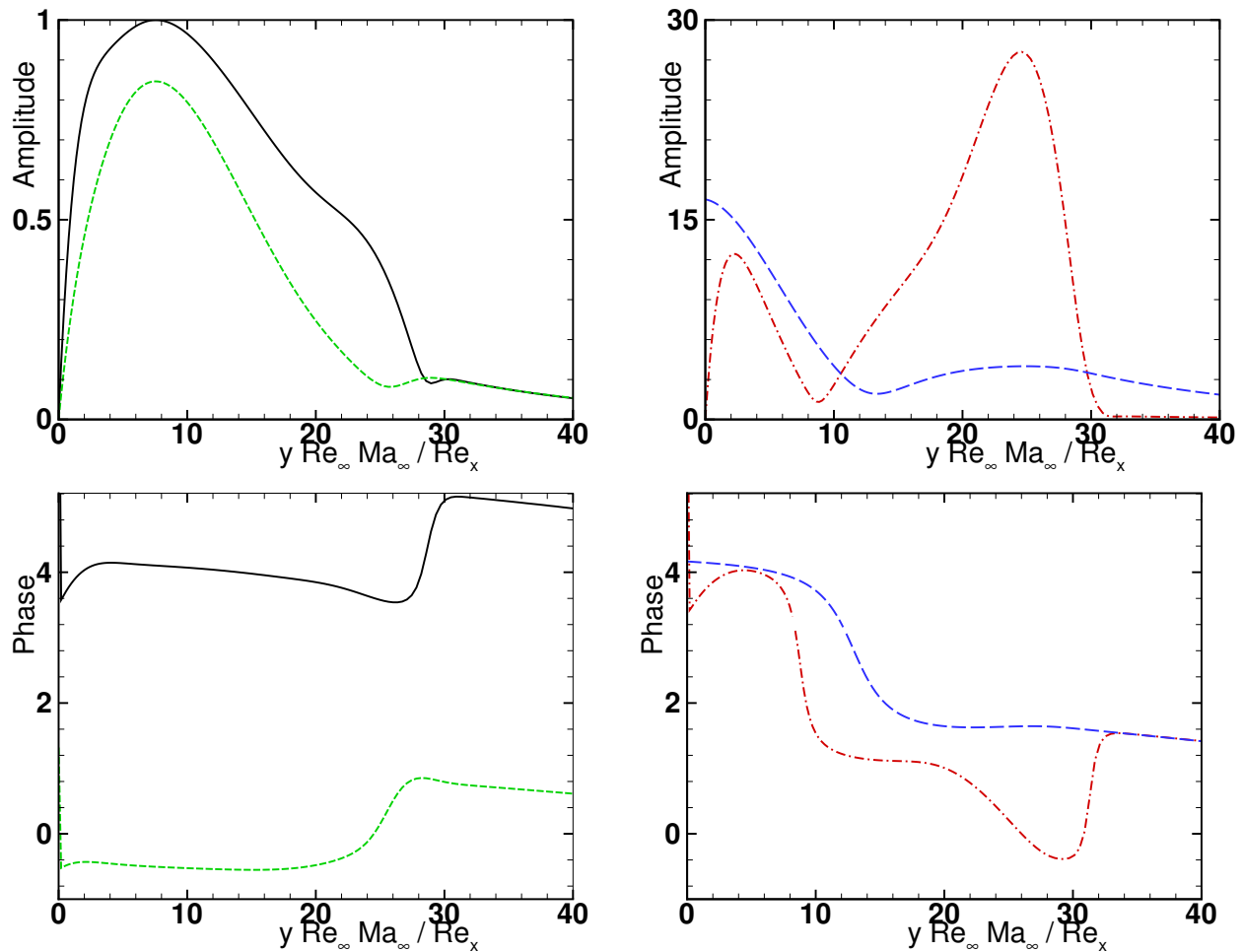


Figure 9: Amplitude (top) and phase (bottom) functions for a second mode disturbance at $Re_x=2000$ from numerical simulation[49], case A, all normalized by the maximum amplitude of the streamwise velocity. Left: streamwise u (solid line) and wall-normal v (dotted line) velocity components. Right: pressure p_5 (dashed line) and temperature T (dash-dotted line).

- [8] Day, M. S. and Bell, J. B., “Numerical simulation of laminar reacting flows with complex chemistry,” *Combust. Theor. Model.*, Vol. 4, 2000, pp. 535–556.
- [9] Nicoud, F., “Conservative High-Order Finite-Difference Schemes for Low-Mach Number Flows,” *J. Comput. Phys.*, Vol. 158, No. 1, 2000, pp. 71–97.
- [10] Hilbert, R., Tap, F., El-Rabii, H., and Thèvenin, D., “Impact of detailed chemistry and transport models on turbulent combustion simulations,” *Prog. Energ. Combust.*, Vol. 30, No. 1, 2004, pp. 61 – 117.
- [11] Najm, H. and Knio, O., “Modeling low Mach number reacting flow with detailed chemistry and transport,” *J. Sci. Comput.*, Vol. 25, 2005, pp. 263–287.
- [12] Zhong, X., “Additive Semi-Implicit Runge-Kutta Methods for Computing High-Speed Nonequilibrium Reactive Flows,” *J. Comput. Phys.*, Vol. 128, No. 1, 1996, pp. 19 – 31.

- [13] Kaneko, M., Men'shov, I., and Nakamura, Y., "Numerical simulation of nonequilibrium flow in high-enthalpy shock tunnel," *Energy*, Vol. 30, No. 2-4, 2005, pp. 165 – 179, 3rd International Symposium on Advanced Energy Conversion Systems and Related Technologies.
- [14] Matheou, G., Pantano, C., and Dimotakis, P. E., "Verification of a fluid-dynamics solver using correlations with linear stability results," *Journal of Computational Physics*, Vol. 227, No. 11, May 2008, pp. 5385–5396.
- [15] Duan, L. and Martín, M. P., "Procedure to Validate Direct Numerical Simulations of Wall-Bounded Turbulence Including Finite-Rate Reactions," *AIAA J*, Vol. 47, No. 1, 2009, pp. 244–251.
- [16] Prakash, A., Parsons, N., Wang, X., and Zhong, X., "High-order shock-fitting methods for direct numerical simulation of hypersonic flow with chemical and thermal nonequilibrium," *Journal of Computational Physics*, Vol. 230, No. 23, Sept. 2011, pp. 8474–8507.
- [17] Coussement, A., Gicquel, O., Caudal, J., Fiorina, B., and Degrez, G., "Journal of Computational Physics," *Journal of Computational Physics*, Vol. 231, No. 17, July 2012, pp. 5571–5611.
- [18] Reshotko, E., "Is Re_{θ}/M_e a Meaningful Transition Criterion?" *AIAA J*, Vol. 45, No. 7, 2007, pp. 1441–1443.
- [19] Reda, D. C., "Review and Synthesis of Roughness-Dominated Transition Correlations for Reentry Applications," *J. Spacecraft Rockets*, Vol. 39, No. 2, 2002, pp. 161–167.
- [20] Malik, M. R., "Prediction and control of transition in supersonic and hypersonic boundary layers," *AIAA J*, Vol. 27, No. 11, Nov. 1989, pp. 1487–1493.
- [21] Berry, S., Daryabeigi, K., Wurster, K., and Bittner, R., "Boundary-Layer Transition on X-43A," *Journal of Spacecraft and Rockets*, Vol. 47, No. 6, 2010, pp. 922–934.
- [22] Reed, H., "Sensitivity and receptivity," *Progress in Flow Instability Analysis and Laminar-Turbulent Transition Modeling*, VKI lecture series, 2014.
- [23] Zhong, X. and Wang, X., "Direct Numerical Simulation on the Receptivity, Instability, and Transition of Hypersonic Boundary Layers," *Annu. Rev. Fluid Mech.*, Vol. 44, No. 1, Jan. 2012, pp. 527–561.
- [24] Ozgen, S., "Linear Stability Theory," *Progress in Flow Instability Analysis and Laminar-Turbulent Transition Modeling*, VKI lecture series, 2014.
- [25] Pinna, F., "Stability of boundary layer flows at different regimes," *Progress in Flow Instability Analysis and Laminar-Turbulent Transition Modeling*, VKI lecture series, 2014.
- [26] Henningson, D., "Non modal stability," *Progress in Flow Instability Analysis and Laminar-Turbulent Transition Modeling*, VKI lecture series, 2014.
- [27] Herbert, T., "Secondary instability of boundary layers," *Ann. Rev. Fluid Mech.*, Vol. 20, 1988, pp. 487–526.
- [28] Kachanov, Y. S. and Levchenko, V. Y., "The resonant interaction of disturbances at laminar-turbulent transition in a boundary layer," *J. Fluid Mech.*, Vol. 138, 1984, pp. 209–247.

- [29] Ho, C.-M. and Huerre, P., "Perturbed Free Shear Layers," *Ann. Rev. Fluid Mech.*, Vol. 16, 1984, pp. 365–424.
- [30] Chang, C.-L. and Malik, M. R., "Oblique-mode breakdown and secondary instability in supersonic boundary layers," *J. Fluid Mech.*, Vol. 273, 1994, pp. 323–360.
- [31] Malik, M. R., "Oblique route to turbulence," *J. Fluid Mech.*, Vol. 674, April 2011, pp. 1–4.
- [32] Mashayek, A. and Peltier, W. R., "The 'zoo' of secondary instabilities precursory to stratified shear flow transition. Part 1 Shear aligned convection, pairing, and braid instabilities," *J. Fluid Mech.*, Vol. 708, Aug. 2012, pp. 5–44.
- [33] Hornung, H. G., "Hypersonic real-gas effects on transition," *IUTAM Symposium on One Hundred Years of Boundary Layer Research*, edited by G. Meier and K. Sreenivasan, Springer, The Netherlands, 2006, pp. 335–344.
- [34] Germain, P. D. and Hornung, H. G., "Transition on a slender cone in hypervelocity flow," *Exp. Fluids*, Vol. 22, 1997, pp. 183–190.
- [35] Malik, M. R. and Anderson, E. C., "Real gas effects on hypersonic boundary-layer stability," *Phys. Fluids A*, Vol. 3, No. 5, 1991, pp. 803–821.
- [36] Stuckert, G. and Reed, H. L., "Linear Disturbances in Hypersonic, Chemically Reacting Shock Layers," *AIAA J.*, Vol. 32, No. 7, 1994, pp. 1384–1393.
- [37] Hudson, M. L., Chokani, N., and Candler, G. V., "Linear Stability of Hypersonic Flow in Thermochemical Nonequilibrium," *AIAA J.*, Vol. 35, No. 6, 1997, pp. 958–964.
- [38] Johnson, H. B., Seipp, T., and Candler, G. V., "Numerical study of hypersonic reacting boundary layer transition on cones," *Phys. Fluids*, Vol. 10, No. 10, 1998, pp. 2676–2685.
- [39] Malik, M. R., "Hypersonic Flight Transition Data Analysis Using Parabolized Stability Equations with Chemistry Effects," *J. Spacecraft Rockets*, Vol. 40, No. 3, 2003, pp. 332–344.
- [40] Klentzman, J., Ulker, E., and Tumin, A., "Projection of the solution of the linearized Navier-Stokes equations in reacting high speed boundary layers onto discrete modes," *42nd AIAA Fluid Dynamics Conference and Exhibit*, No. AIAA 2012-3149, 2012, pp. 1–19.
- [41] Franko, K. J., MacCormack, R. W., and Lele, S. K., "Effects of Chemistry Modeling on Hypersonic Boundary Layer Linear Stability Prediction," *AIAA Paper*, Vol. 2010–4601, 2010.
- [42] Johnson, H. B. and Candler, G. V., "Hypersonic Boundary Layer Stability Analysis Using PSE-Chem," *AIAA Paper*, Vol. 2005–5023, 2005.
- [43] Chang, C.-L., Vinh, H., and Malik, M. R., "Hypersonic Boundary-Layer Stability with Chemical Reactions using PSE," *AIAA Paper*, Vol. 97–2012, 1997.
- [44] Liu, Y. and Vinokur, M., "Nonequilibrium Flow Computations. I. An Analysis of Numerical Formulations of Conservation Laws," *J. Comput. Phys.*, Vol. 83, 1989, pp. 373–397.

- [45] Candler, G. V. and Nompelis, I., “Computational Fluid Dynamics for Atmospheric Entry,” *RTO-EN-AVT-162 Non-Equilibrium Gas Dynamics – From Physical Models to Hypersonic Flights*, van Karman Institut, Rhode-Saint-Genese, Belgium, 2009, pp. 15.1–15.56.
- [46] Ma, Y. and Zhong, X., “Receptivity to Freestream Disturbances of a Mach 10 Nonequilibrium Reacting Oxygen Flow over A Flat Plate,” *AIAA Paper*, Vol. 2004–0256, 2004.
- [47] Parsons, N., Zhong, X., Kim, J., and Eldredge, J., “Numerical Study of Hypersonic Receptivity with Thermochemical Non-Equilibrium on a Blunt Cone,” *AIAA Paper*, Vol. 2010–4446, 2010.
- [48] Marxen, O., Magin, T., Iaccarino, G., and Shaqfeh, E. S. G., “A high-order numerical method to study hypersonic boundary-layer instability including high-temperature gas effects,” *Phys. Fluids*, Vol. 23, No. 8, 2011, pp. 084108.
- [49] Marxen, O., Magin, T., Shaqfeh, E. S. G., and Iaccarino, G., “A method for the direct numerical simulation of hypersonic boundary-layer instability with finite-rate chemistry,” *J. Comp. Phys.*, Vol. 255, 2013, pp. 572–589.
- [50] Marxen, O., Iaccarino, G., and Magin, T., “Direct numerical simulation of hypersonic boundary-layer transition with finite-rate chemistry,” *J. Fluid Mech.*, Vol. 755, May 2014, pp. 35–49.
- [51] Reshotko, E. and Tumin, A., “Role of Transient Growth in Roughness-Induced Transition,” *AIAA J.*, Vol. 42, No. 4, April 2004, pp. 766–770.
- [52] Hanifi, A., Schmid, P. J., and Henningson, D. S., “Transient growth in compressible boundary layer flow,” *Phys. Fluids*, Vol. 8, No. 3, 1996, pp. 826.
- [53] Tumin, A. and Reshotko, E., “Optimal Disturbances in Compressible Boundary Layers,” *AIAA J.*, Vol. 41, No. 12, Dec. 2003, pp. 2357–2363.
- [54] Zuccher, S., Tumin, A., and Reshotko, E., “Parabolic approach to optimal perturbations in compressible boundary layers,” *J. Fluid Mech.*, Vol. 556, May 2006, pp. 189–216.
- [55] Mack, L. M., “Boundary layer stability theory,” Tech. Rep. JPL-900-277-REV-A; NASA-CR-131501, Jet Propulsion Laboratory, NASA, 1969.
- [56] Fedorov, A. V., “Transition and Stability of High-Speed Boundary Layers,” *Annu. Rev. Fluid Mech.*, Vol. 43, 2011, pp. 79–95.
- [57] Tumin, A., “Three-dimensional spatial normal modes in compressible boundary layers,” *J. Fluid Mech.*, Vol. 586, 2007, pp. 295–322.
- [58] Fedorov, A. and Tumin, A., “High-Speed Boundary-Layer Instability: Old Terminology and a New Framework,” *AIAA J.*, Vol. 49, No. 8, Aug. 2011, pp. 1647–1657.
- [59] Marxen, O., Lang, M., and Rist, U., “Discrete linear local eigenmodes in a separating laminar boundary layer,” *J. Fluid Mech.*, Vol. 711, 2012, pp. 1–26.
- [60] Pagella, A., Rist, U., and Wagner, S., “Numerical investigations of small-amplitude disturbances in a boundary layer with impinging shock wave at $Ma=4.8$,” *Phys. Fluids*, Vol. 14, No. 7, 2002, pp. 2088–2100.

- [61] Lifshitz, Y., Degani, D., and Tumin, A., “Study of Discrete Modes Branching in High-Speed Boundary Layers,” *AIAA J.*, Vol. 50, No. 10, 2012, pp. 2202–2210.
- [62] Herbert, T., “Parabolized stability equations,” *Ann. Rev. Fluid Mech.*, Vol. 29, No. 1, 1997, pp. 245–283.
- [63] Tollmien, W., “Über die Entstehung der Turbulenz. 1. Mitteilung,” 1929, pp. 21–44, English translation: The production of turbulence, NACA TM-609 (1931).
- [64] Schlichting, H., “Zur Entstehung der Turbulenz bei der Plattenströmung,” *Nachr. d. Ges. d. Wiss. zu Göttingen, Math.-Phys. Klasse*, 1933, pp. 181–208, also *ZAMM* **13** (3), 171–174.
- [65] Schmid, P. J. and Henningson, D. S., *Stability and Transition in Shear Flows*, Springer, Berlin, New York, 1st ed., 2001.
- [66] Schubauer, G. B. and Skramstad, H. K., “Laminar Boundary-Layer Oscillations and Stability of Laminar Flow,” *J. Aeronaut. Sci.*, Vol. 14, No. 2, 1947, pp. 69–78.
- [67] Rayleigh, L., “On the stability, or instability, of certain fluid motions,” *Proc. Lond. Math. Soc.*, Vol. 11, 1880, pp. 57–70.
- [68] Rayleigh, L., “On the stability, or instability, of certain fluid motions, II,” *Proc. Lond. Math. Soc.*, Vol. 19, 1887, pp. 67–74.
- [69] Lees, L. and Lin, C., “Investigation of the instability of the laminar boundary layer in a compressible fluid,” Tech. Rep. 1115, NACA, 1946.
- [70] Mack, L. M., “Linear Stability Theory and the Problem of Supersonic Boundary-Layer Transition,” *AIAA J.*, Vol. 13, No. 3, 1975, pp. 278–2285.
- [71] Mack, L. M., “Boundary-Layer Linear Stability Theory,” Tech. Rep. 709, AGARD Report, Special course on stability and transition of laminar flow, 1984.
- [72] Arnal, D., “Boundary layer transition,” *Special Course on Progress in Transition Modelling*, No. R-793, AGARD, 1994.
- [73] Kachanov, Y. S., “Physical Mechanisms of Laminar-Boundary-Layer Transition,” *Ann. Rev. Fluid Mech.*, Vol. 26, No. 1, Jan. 1994, pp. 411–482.
- [74] Reed, H. L., Saric, W. S., and Arnal, D., “Linear Stability Theory Applied to Boundary Layers,” *Ann. Rev. Fluid Mech.*, Vol. 28, No. 1, Jan. 1996, pp. 389–428.
- [75] Marxen, O., Iaccarino, G., and Shaqfeh, E. S. G., “Disturbance evolution in a Mach 4.8 boundary layer with two-dimensional roughness-induced separation and shock,” *J. Fluid Mech.*, Vol. 648, 2010, pp. 435–469.
- [76] Marxen, O., Iaccarino, G., and Shaqfeh, E. S. G., “Nonlinear instability of a supersonic boundary layer with two-dimensional roughness,” *J. Fluid Mech.*, Vol. 752, July 2014, pp. 497–520.
- [77] Johnson, H. B., Gronvall, J. E., and Candler, G. V., “Reacting Hypersonic Boundary Layer Stability with Blowing and Suction,” *47th AIAA Aerospace Sciences Meeting, Orlando, Florida*, No. 2009–938, 2009.

- [78] Ghaffari, S., Marxen, O., Iaccarino, G., and Shaqfeh, E. S. G., “Numerical simulations of hypersonic boundary-layer instability with wall blowing,” *48th AIAA Aerospace Sciences Meeting Including the New Horizons Forum and Aerospace Exposition, Orlando, Florida*, No. 2010–706, 2010.
- [79] Stetson, K. F., Thompson, E. R., Donaldson, J. C., and Siler, L. G., “Laminar Boundary-Layer Stability Experiments on a Cone at Mach 8, Part 1: Sharp Cone,” *AIAA Paper*, Vol. 83–1761, 1983.
- [80] Reed, H., “Role of Chemical Reactions in Hypersonic Flows,” *RTO-EN-AVT-151 Advances in Laminar-Turbulent Transition Modelling*, van Karman Institut, Rhode-Saint-Genese, Belgium, 2009, pp. 13.1–13.15.
- [81] Fujii, K. and Hornung, H. G., “Experimental Investigation of High-Enthalpy Effects on Attachment-Line Boundary-Layer Transition,” *AIAA Journal*, Vol. 41, No. 7, July 2003, pp. 1282–1291.
- [82] Ma, Y. and Zhong, X., “Receptivity of a supersonic boundary layer over a flat plate. Part 1. Wave structures and interactions,” *Journal of Fluid Mechanics*, Vol. 488, July 2003, pp. 31–78.